
Gaussian Process Priors for Systems of Linear Partial Differential Equations with Constant Coefficients

Marc Härkönen

Max Planck Institute for Mathematics in the Sciences
marc.harkonen@gmail.com

Markus Lange-Hegermann

Institute industrial IT
OWL University of Applied Sciences and Arts
markus.lange-hegermann@th-owl.de

Bogdan Raiță

Centro di Ricerca Matematica Ennio de Giorgi
Scuola Normale Superiore di Pisa
bogdanrait@gmail.com

Abstract

Partial differential equations (PDEs) are important tools to model physical systems, and including them into machine learning models is an important way of incorporating physical knowledge. Given any system of linear PDEs with constant coefficients, we propose a family of Gaussian process (GP) priors, which we call EPGP, such that all realizations are exact solutions of this system. We apply the Ehrenpreis-Palamodov fundamental principle, which works like a non-linear Fourier transform, to construct GP kernels mirroring standard spectral methods for GPs. Our approach can infer probable solutions of linear PDE systems from any data such as noisy measurements, or initial and boundary conditions. Constructing EPGP-priors is algorithmic, generally applicable, and comes with a sparse version (S-EPGP) that learns the relevant spectral frequencies and works better for big data sets. We demonstrate our approach on three families of systems of PDE, the heat equation, wave equation, and Maxwell's equations, where we improve upon the state of the art in computation time and precision, in some experiments by several orders of magnitude.

1 Introduction

Gaussian processes (GPs) [1] are a major tool in probabilistic machine learning and serve as the default functional prior in Bayesian statistics. GPs are specified by a mean function and a covariance function. Especially the covariance function can be constructed flexibly to allow various kinds of priors [2] and learning hyperparameters in GPs allows to interpret data [3–5]. They serve as stable regression models in applications with few data points and provide calibrated variances of predictions. In particular, they can serve as simulation models for costly to evaluate functions, e.g. in Bayesian optimization [6] or active learning [7]. Furthermore, GPs are often the models of choice to encode mathematical information in a prior or if mathematical results should be extracted from a model. One example is the estimation of derivatives from data by differentiating the covariance function [8, 9].

These techniques using derivatives have been generalized to construct GPs with realizations in the solution set of specific systems of linear partial differential equations (PDEs) with constant coefficients [10–15]. These constructions interpret such a solution set as the image of some latent functions under a linear operator matrix. Assuming a GP prior for these latent function leads to a GP prior for the solution set of the system of PDEs. The paper [16] pointed out that these constructions of GP priors had striking similarities and suggested an approach for a general construction, after which [17] reinterpreted this approach in terms of Gröbner bases and made it algorithmic. One limitation was

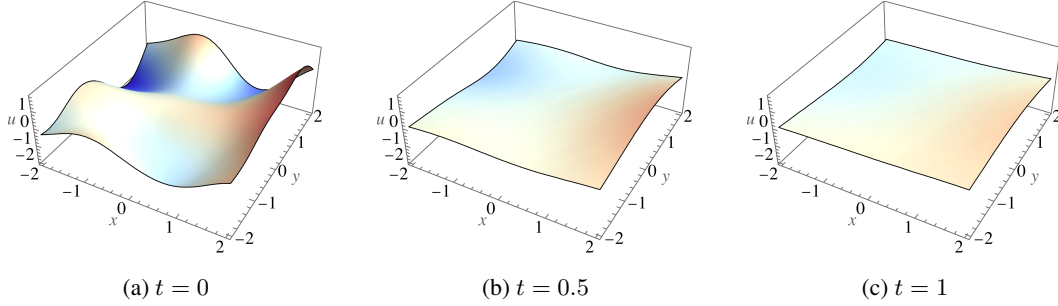


Figure 1: Sample of a function $u(x, y, t)$ describing the temperature of a 2-dimensional material over time. The sample is obtained using the EPGP covariance kernel solving the heat equation in 2D. We observe the dissipation of heat as time progresses.

that the method could only work on a subclass of systems of linear PDEs with constant coefficients: the so-called controllable (or parametrizable) systems. The restriction to such controllable systems was lifted for systems of ordinary differential equations (ODEs) in [18].

In this paper, we develop an algorithmic construction of GP priors inside *any* given system of (ordinary or partial) linear differential equations with constant coefficients, without restriction to special forms of equations, controllable systems, or ODEs. Our construction is built upon the classical Ehrenpreis-Palamodov fundamental principle (see Section 3) and recent algorithms for the construction of Noetherian multipliers used in this theorem [19–23]. The major contributions of this paper are as follows:

1. We *vastly generalize* previously isolated methods to model systems of ODEs and PDEs from data, such that only the restrictions of linearity and constant coefficients remain, and reinterpret the previously existing methods in our framework.
2. We demonstrate our approach on various systems of equations, in particular the *homogeneous* Maxwell equations, see Section 6.3.
3. We demonstrate high accuracy of our approach, clearly beating state of the art Physics Informed Neural Network (PINN) methods in several examples (see Section 6).

Hence, this paper allows the application of machine learning techniques for a vast class of differential equations ubiquitous in physics and numerical analysis. In particular, we propose a symbolic framework for turning physical knowledge from differential equations into a form usable in machine learning. The symbolic approach allows us to sample and regress on *exact* solutions of the PDE system, making our methods not merely physics *informed*, but truly physics *constrained*. Therefore, our GPs result in more precise regression models, since they do not need to use information present in the data or additional collocation points to learn or fit to the differential equation, and instead can use the full information content of the data to build upon the known differential equations.

2 Gaussian processes (GPs)

A *Gaussian process (GP)* $g \sim \text{GP}(\mu, k)$ defines a probability distribution on the evaluations of functions $\Omega \rightarrow \mathbb{R}^\ell$, where $\Omega \subseteq \mathbb{R}^n$, such that function values $g(x_1), \dots, g(x_m)$ at any points $x_1, \dots, x_m \in \Omega$ are jointly Gaussian. A GP g is specified by a *mean function* $\mu : \Omega \rightarrow \mathbb{R}^\ell : x \mapsto \mathbb{E}[g(x)]$, often a-priori chosen to be zero, and a positive semidefinite, smooth *covariance function*

$$k : \Omega \times \Omega \longrightarrow \mathbb{R}_{\geq 0}^{\ell \times \ell} : (x, x') \longmapsto \mathbb{E}[(g(x) - \mu(x))(g(x') - \mu(x'))^T].$$

Then, any finite set of evaluations of g follows the multivariate Gaussian distribution

$$\begin{bmatrix} g(x_1) \\ \vdots \\ g(x_m) \end{bmatrix} \sim \mathcal{N} \left(\begin{bmatrix} \mu(x_1) \\ \vdots \\ \mu(x_m) \end{bmatrix}, \begin{bmatrix} k(x_1, x_1) & \dots & k(x_1, x_m) \\ \vdots & \ddots & \vdots \\ k(x_m, x_1) & \dots & k(x_m, x_m) \end{bmatrix} \right).$$

Due to the properties of Gaussian distributions, the posterior is again a GP and can be computed in closed form via linear algebra [1].

GPs interplay nicely with linear operators, the foundation of the constructions of [10–18, 24, 25]:

Lemma 2.1. *Let $g \sim \text{GP}(\mu(x), k(x, x'))$ with realizations in some function space \mathcal{F}^ℓ and $B : \mathcal{F}^\ell \rightarrow \mathcal{G}^{\ell''}$ a linear, measurable operator. Then, the pushforward B_*g of g under B is a GP with*

$$B_*g \sim \text{GP}(B\mu(x), Bk(x, x')(B')^T), \quad (1)$$

where B' denotes the operation of B on functions with argument x' .

We prove this lemma in Appendix A.

Let $\mathcal{F} = C^\infty(\Omega, \mathbb{R})$ the space of smooth function on $\Omega \subset \mathbb{R}^d$. The squared exponential covariance function $k_{\mathcal{F}}(x, x') = \exp(-\frac{1}{2}(x - x')^2)$ induces a GP prior with realizations contained in \mathcal{F} .

3 The Ehrenpreis-Palamodov fundamental principle

Consider the familiar case of a linear ODE with constant coefficients, e.g. $f'''(x) - 3f'(x) + 2f(x) = 0$. Its *characteristic polynomial* $z^3 - 3z + 2$ determines the solution space of the ODE via the roots of the characteristic polynomial and their multiplicities. In this case, since $z^3 - 3z + 2$ factors into $(z - 1)^2 \cdot (z - (-2))$, all solutions are linear combinations of the three functions e^{1x} , $x \cdot e^{1x}$ and e^{-2x} . We call functions of the form $D(x) \cdot e^{zx}$ *exponential-polynomial* functions whenever $D(x)$ is a polynomial and z is a constant. This idea generalizes to systems of ODEs and PDEs: instead of taking linear combinations of exponential-polynomial functions over finitely many zeroes of the characteristic polynomial, one takes a weighted integral of exponential-polynomial functions over a (potentially multi-dimensional) characteristic variety, i.e. the solution set of a system of polynomial equations. This generalization is formalized in the Ehrenpreis-Palamodov fundamental principle, Theorem 3.1.

More formally, let Ω be a compact, convex subset of \mathbb{R}^n . Consider systems of ℓ equations with smooth functions $f : \Omega \rightarrow \mathbb{C}^{\ell''}$ as potential solutions. We encode such a system of PDE as an $(\ell \times \ell'')$ matrix A with entries in the polynomial ring $R = \mathbb{C}[\partial_1, \dots, \partial_n]$ in n variables. Here the symbol ∂_i encodes the operator $\frac{\partial}{\partial x_i}$, and a monomial $\partial^\alpha = \partial_1^{\alpha_1} \dots \partial_n^{\alpha_n}$ denotes the operator $\frac{\partial^{|\alpha|}}{\partial x_1^{\alpha_1} \dots \partial x_n^{\alpha_n}}$. For example, for $\ell = 3$, $\ell'' = 2$, $n = 2$, the PDE system

$$Af = \begin{bmatrix} \partial_1 & -\partial_1\partial_2 \\ \partial_2 + 2 & 0 \\ \partial_1^2\partial_2 & -\partial_1 + 3\partial_2 \end{bmatrix} f = \begin{bmatrix} \frac{\partial f_1}{\partial x_1} - \frac{\partial^2 f_2}{\partial x_1 \partial x_2} \\ \frac{\partial f_1}{\partial x_2} + 2f_1 \\ \frac{\partial^3 f_1}{\partial x_1^2 \partial x_2} - \frac{\partial f_2}{\partial x_1} + 3\frac{\partial f_2}{\partial x_2} \end{bmatrix} = 0$$

consists of 3 homogeneous equations describing a vector valued function $f(x_1, x_2) = (f_1(x_1, x_2), f_2(x_1, x_2))^T$.

The famed Ehrenpreis-Palamodov fundamental principle asserts that all solutions to the PDE represented by A can be written as suitable *integrals* of exponential-polynomial functions, each of which corresponds to roots and multiplicities of the polynomial module generated by rows of A .

Theorem 3.1. (Ehrenpreis, Palamodov, [26–29]) *Let $A \in R^{\ell \times \ell''}$ and let $\Omega \subseteq \mathbb{R}^n$ be a convex, compact set. There exist algebraic varieties $\{V_1, \dots, V_s\}$ and ℓ'' -tuples of polynomials $\{D_{i,1}(\mathbf{x}, \mathbf{z}), \dots, D_{i,m_i}(\mathbf{x}, \mathbf{z})\}_{i=1, \dots, s}$ such that any smooth solution $f : \Omega \rightarrow \mathbb{R}^{\ell''}$ to the equation $Af = 0$ can be written as*

$$f(\mathbf{x}) = \sum_{i=1}^s \sum_{j=1}^{m_i} \int_{V_i} D_{i,j}(\mathbf{x}, \mathbf{z}) e^{\langle \mathbf{x}, \mathbf{z} \rangle} d\mu_{i,j}(\mathbf{z}) \quad (2)$$

for a suitable choice of measures $\mu_{i,j}$.

Following the terminology in [20, 21], we call the polynomials $D_{i,j}(\mathbf{x}, \mathbf{z})$ *Noetherian multipliers*. The Noetherian multipliers $D_{i,j}$ and varieties V_i appearing in Theorem 3.1 can be computed algebraically; they are the higher-dimensional analogue of the roots and multiplicities of the characteristic

polynomial. An algorithm for computing $D_{i,j}$ and V_i is implemented under the command `solvePDE` in the Macaulay2 [30] package `NotherianOperators` [19]. A modern, algebraic and algorithmic treatment of linear PDE with constant coefficients can be found in [20–23]. We refer the interested reader to Appendix B for questions regarding convergence of the integrals in (2).

4 Gaussian Process Priors from the Ehrenpreis-Palamodov Theorem

We now construct GPs whose samples solve a system of linear PDEs A , using the Ehrenpreis-Palamodov fundamental principle 3.1. We set the mean function $\mu(\mathbf{x}) = 0$, so our task, by Lemma 2.1, will be to find a covariance function that satisfies the PDE in both the \mathbf{x} and \mathbf{x}' arguments. The varieties V_i and polynomials D_i in eq. (2) can be computed algorithmically [19–23], so what remains is to choose the measures $\mu_{i,j}$, each supported on the variety V_i .

We propose two approaches for choosing the measures. In the first one, coined Ehrenpreis-Palamodov Gaussian Process (EPGP), the $\mu_{i,j}$ are chosen to be Gaussian measures supported on the variety, with optional trainable length scale and shift parameters. This mirrors [31], but applied to Ehrenpreis-Palamodov integrals as opposed to Fourier transforms. Our second approach, Sparse Ehrenpreis-Palamodov Gaussian Process (S-EPGP), chooses $\mu_{i,j}$ to be linear combinations of Dirac delta measures, whose locations and weights can be learned. See [32] for a similar approach applied to Fourier transforms.

Before describing our covariance functions, we discuss the question of how to integrate over an algebraic variety. In certain cases our variety has a polynomial parametrization, in which case the integral can easily be computed by substituting the parametrization in. For example if V is the variety corresponding to the parabola $y = x^2$, we can rewrite an integral $\int_V f(x, y) d\mu(x, y)$ over V as $\int_{\mathbb{C}} f(x, x^2) d\mu'(x)$.

However, most algebraic varieties V do not have an “obvious” parametrization. In these cases we construct a parametrization implicitly by solving equations. If for example the variety V is the set of points (x, y, z) where $x^3 - y^2 + z^2 = 0$, we could solve for z to get $z = \pm\sqrt{y^2 - x^3}$. Thus, an integral of the form $\int_V f(x, y, z) d\mu(x, y, z)$ can be rewritten as a sum $\int_{\mathbb{C}^2} f(x, y, \sqrt{y^2 - x^3}) d\mu_1(x, y) + \int_{\mathbb{C}^2} f(x, y, -\sqrt{y^2 - x^3}) d\mu_2(x, y)$ of integrals over \mathbb{C}^2 . This construction works for arbitrary varieties $V \subseteq \mathbb{C}^n$, and relies on results in algebraic dimension theory. We now cite the main results and refer to e.g. [33, Sec. 13.1] for a comprehensive treatment of the subject.

Suppose we denote the coordinates of \mathbb{C}^n by z_1, \dots, z_n . If V has dimension d , there is a set of d independent variables, say $\mathbf{z}' = (z_1, \dots, z_d)$ after reordering our coordinates, on which the remaining variables $\mathbf{z}'' = (z_{d+1}, \dots, z_n)$ depend polynomially. Thus for each choice of \mathbf{z}' , there is a finite number of \mathbf{z}'' such that $\mathbf{z} = (\mathbf{z}', \mathbf{z}'') \in V$. We denote this set by $\mathcal{S}_{\mathbf{z}'} := \{\mathbf{z} \in V : (z_1, \dots, z_d) = \mathbf{z}'\}$. Using this notation, an integral $\int_V f(\mathbf{z}) d\mu(\mathbf{z})$ over V can now be rewritten as an integral $\int_{\mathbb{C}^d} \sum_{\mathbf{z} \in \mathcal{S}_{\mathbf{z}'}} f(\mathbf{z}) d\mu(\mathbf{z}')$ over the much easier to handle affine space \mathbb{C}^d , at the cost of changing the measure and splitting our integral into several pieces.

4.1 Ehrenpreis-Palamodov Gaussian Processes (EPGP)

Let $A(\partial)$ be a system of PDE whose solutions are, by Ehrenpreis-Palamodov, of the form $\phi(\mathbf{x}) = \sum_j \int_V D_j(\mathbf{x}, \mathbf{z}) e^{\langle \mathbf{x}, \mathbf{z} \rangle} d\mu_j(\mathbf{z})$. We define the EPGP kernel $k_{\text{EPGP}}(\mathbf{x}, \mathbf{x}')$ by combining the Ehrenpreis-Palamodov representation in both inputs \mathbf{x}, \mathbf{x}' , the above implicit parametrization of the integrals, and a Gaussian measure on the base space. We construct one covariance kernel for each summand in $\phi(\mathbf{x})$ and sum them to get the EPGP kernel k_{EPGP} :

$$\begin{aligned} \Psi(\mathbf{x}, \mathbf{z}') &:= \sum_j \sum_{\mathbf{z} \in \mathcal{S}_{\mathbf{z}'}} D_j(\mathbf{x}, \mathbf{z}) e^{\langle \mathbf{x}, \mathbf{z} \rangle} \\ k_{\text{EPGP}}(\mathbf{x}, \mathbf{x}') &:= \int_{\mathbf{z}' \in \sqrt{-1}\mathbb{R}^d} \Psi(\mathbf{x}, \mathbf{z}') \Psi(\mathbf{x}', \mathbf{z}')^H e^{-\frac{\|\mathbf{z}'\|^2}{2}} d\mathcal{L}(\mathbf{z}'), \end{aligned} \quad (3)$$

where the superscript H denotes the Hermitian transpose, and \mathcal{L} is the usual Lebesgue measure. We note that the integral may not converge everywhere, but we can introduce a shifting term to enforce

convergence in any compact set Ω . See Appendix B for details. It is straightforward to check that $k_{\text{EPGP}}(\mathbf{x}, \mathbf{x}')$ satisfies the PDEs in A , and the Hermitian transpose ensures that k_{EPGP} is positive semidefinite. A strictly real valued GP is obtained by taking the real part of k_{EPGP} .

The integral over the complex space $\mathbf{z}' \in \mathbb{C}^d$ is replaced by an integral over purely imaginary vectors $\mathbf{z}' \in \sqrt{-1}\mathbb{R}$. We motivate this choice, and the choice of the Gaussian measure, in three examples:

Example 4.1 (No PDE). If $A(\partial) = 0$ is zero, we impose no PDE constraints. In this case, we have one variety $V = \mathbb{C}^n$ and one Noetherian multiplier $D(\mathbf{x}, \mathbf{z}) = 1$, so equation (3) becomes

$$k_{\text{EPGP}}(\mathbf{x}, \mathbf{x}') = \int_{\mathbf{z} \in \mathbb{R}} e^{\sqrt{-1}\langle \mathbf{x} - \mathbf{x}', \mathbf{z} \rangle} e^{-\frac{\|\mathbf{z}\|^2}{2}} d\mathcal{L}(\mathbf{z}) = \sqrt{2\pi}^n e^{-\frac{\|\mathbf{x} - \mathbf{x}'\|^2}{2}}$$

Thus, without PDEs, the EPGP kernel is the squared-exponential kernel, up to a constant scaling.

The discussion in this example extends to any system of PDE A whose characteristic variety V is an affine subspace of \mathbb{C}^n . For details, refer to Appendix G. \triangle

Example 4.2 (Heat equation). Let $A(\partial_x, \partial_t) = \partial_x^2 - \partial_t$ be the one-dimensional heat equation. If we let z_1, z_2 correspond to ∂_x, ∂_t respectively, the variety V is given by $z_1^2 = z_2$, and the sole Noetherian multiplier is $D = 1$. The EPGP kernel is defined when $t + t' > -\frac{1}{2}$, in which case we have

$$k_{\text{EPGP}}(x, t; x', t') = \int_{z \in \mathbb{R}} e^{\sqrt{-1}(x-x')z} e^{-z^2(t+t')} e^{-\frac{z^2}{2}} d\mathcal{L}(z) = \sqrt{2\pi} \frac{e^{-\frac{(x-x')^2}{2(1+2(t+t'))}}}{\sqrt{1+2(t+t')}}}$$

In this example, integrating over $\sqrt{-1}\mathbb{R}$ as opposed to \mathbb{C} removes unphysical solutions to the heat equation, such as $\phi(x, t) = e^{x+t}$ where heat increases exponentially with time. \triangle

Example 4.3 (Wave equation). Let $A(\partial_x, \partial_t) = \partial_x^2 - \partial_t^2$ be the 1-dimensional wave equation. The variety here is the set $z_1^2 - z_2^2 = 0$, which is the union of the lines $z_1 = z_2$ and $-z_1 = z_2$. Thus we have $V_j = V(z_1 + (-1)^j z_2)$ and $D_j = 1$ for $j = 1, 2$. We now get the kernel

$$\begin{aligned} k_{\text{EPGP}}(x, t; x', t') &= \int_{z \in \mathbb{R}} \left(e^{\sqrt{-1}z(x-t)} + e^{\sqrt{-1}z(x+t)} \right) \left(e^{-\sqrt{-1}z(x'-t')} + e^{\sqrt{-1}z(x'+t')} \right) e^{-\frac{z^2}{2}} d\mathcal{L}(z) \\ &= \sqrt{2\pi} \left(e^{-\frac{((x-t)-(x'-t'))^2}{2}} + e^{-\frac{((x-t)-(x'+t'))^2}{2}} + e^{-\frac{((x+t)-(x'-t'))^2}{2}} + e^{-\frac{((x+t)-(x'+t'))^2}{2}} \right) \end{aligned}$$

Here our choice of restricting to integrals over strictly imaginary numbers $\sqrt{-1}\mathbb{R}$ gets rid of non-stable solutions to the wave equations, such as e^{x+t} .

While k_{EPGP} has four summands, we can also consider kernels with fewer summands. E.g.

$$k_2(x, t; x', t') = \sqrt{2\pi} e^{-\frac{((x+t)-(x'+t'))^2}{2}} + \sqrt{2\pi} e^{-\frac{((x-t)-(x'-t'))^2}{2}},$$

yields the covariance kernel of the GP $\phi_1(x+t) + \phi_2(x-t)$, where $\phi_1, \phi_2 \sim GP(0, e^{-\frac{(x-x')^2}{2}})$. This kernel in fact covers all smooth solutions to the 1-D wave equation, as d'Alembert discovered in 1747 [34] that all solutions are superpositions of waves travelling in opposite directions. \triangle

Here we have tacitly assumed that the Ehrenpreis-Palamodov integral requires only one variety V , i.e. $s = 1$. In the general case $s > 1$, we repeat the above construction for each variety V_i , and finally sum the resulting s kernels.

We note that we may also parametrize the Gaussian measure imposed in eq. (3), for example with mean and scale parameters. By replacing $\exp(-\frac{\|\mathbf{z}\|^2}{2})$ by e.g. $\exp(-\sum_{i=1}^d \frac{(z_i - \mu_i)^2}{2\sigma_i^2})$, we obtain a family of EPGP kernels, which we can train on given data to find the parameters maximizing the log-marginal likelihood. In the case of no PDE constraints, we recover exactly the covariance kernels proposed in [31]. In Figure 3 of Section 6.1 we investigate the effect of a scale parameter in the posterior distribution of a solution to the 2 dimensional heat equation.

4.2 Sparse Ehrenpreis-Palamodov Gaussian Processes (S-EPGP)

Instead of imposing the measure $e^{-\|\mathbf{z}'\|^2/2} d\mathcal{L}(\mathbf{z}')$ in our kernel, we outline a computationally efficient method for estimating the integral by a weighted sum. The kernels described in this section mirror the

ones in [32], but using representations of PDE solutions via the Ehrenpreis-Palamodov fundamental principle as opposed to the Fourier transform. For notational simplicity we assume that the $D_j(\mathbf{x}, \mathbf{z})$ are scalar values and there is only one variety in eq. (2), i.e. $s = 1$; the extension of our analysis to the general case is straight forward, and a concrete example of S-EPGP applied to Maxwell’s equations can be seen in Section 6.3.

The main idea is to choose the measures $\mu_{i,j}$ in eq. (2) as linear combinations of Dirac delta functions. Ideally we would define a GP prior whose realizations are functions of the form

$$f(\mathbf{x}) = \sum_{j=1}^m \sum_{i=1}^r w_{i,j} D_j(\mathbf{x}, \mathbf{z}_{i,j}) e^{\langle \mathbf{x}, \mathbf{z}_{i,j} \rangle},$$

where all $z_{i,j} \in V$. We would then, given training data, choose $\mathbf{z}_{i,j}$ as to maximize the log marginal likelihood. Unfortunately, the requirement $\mathbf{z}_{i,j} \in V$ makes it challenging to directly use a gradient descent based optimization method.

Instead, we use the implicit parametrization trick from the beginning of this section and are looking at a GP with realizations of the form

$$f(\mathbf{x}) = \sum_{j=1}^m \sum_{i=1}^r w_{i,j} \frac{1}{|S_{\mathbf{z}'_{i,j}}|} \left(\sum_{\mathbf{z} \in S_{\mathbf{z}'_{i,j}}} D_j(\mathbf{x}, \mathbf{z}) e^{\langle \mathbf{x}, \mathbf{z} \rangle} \right) =: \mathbf{w}^T \phi(\mathbf{x}),$$

where now $\mathbf{z}'_{i,j} \in \mathbb{C}^d$, $d = \dim V$, and $\mathbf{w}, \phi(\mathbf{x})$ are vectors of length mr . For the same reasons as in the previous section we usually will choose $\mathbf{z}'_{i,j} \in \sqrt{-1}\mathbb{R}^d$. To turn $f(\mathbf{x})$ into a GP, set $w_{i,j} \sim \mathcal{N}(0, \frac{1}{mr}\Sigma)$, where Σ is a diagonal matrix with positive entries σ_i^2 for $i = 1, \dots, mr$. We then get a covariance function of the form

$$k_{\text{S-EPGP}}(\mathbf{x}, \mathbf{x}') = \frac{1}{mr} \phi(\mathbf{x})^H \Sigma \phi(\mathbf{x}')$$

where $\phi(\mathbf{x})^H$ denotes the conjugate transpose of $\phi(\mathbf{x})$. For computational details on S-EPGP we refer to Appendix C.

5 Comparison to the Literature

Physics informed methods in machine learning systems are a central research topic in deep learning and GPs. The approaches in deep learning often add additional loss terms from the differential equations at pseudo-points, sometimes combined with feature engineering, specific network structures, usage of symmetries and similar techniques. For example, amongst many, see [35–39]. These techniques also include GPs as a technical tool, e.g. [40] uses GPs to estimate solutions of a single PDE, where the derivatives of GPs are being used to construct a loss functions incorporating the PDE, and [41] uses GPs to model a single function constrained by a single linear PDE.

The approaches in [10–17, 42–44] construct GPs for a certain subset of systems of linear partial differential equations with constant coefficients: systems that are controllable. In the language of our paper, the controllable systems are the systems where the characteristic variety has the full space of frequencies as its only primary component, see Appendix G. While [17] offered a method to check whether a system is controllable, the class of such systems is comparatively small. The paper [18] was able to construct priors for all systems of linear ODEs with constant coefficients by using the Smith form to split apart the embedded components in the characteristic variety as direct summands and model the controllable summand via parametrization as in [16, 17] and the (necessarily finite dimensional) uncontrollable summands via linear regression. A special case of these approaches has been used in [45, 46] to construct GP models for systems of linear PDEs with forcing terms; such systems are controllable. Special cases of these approaches have been used in [47] to construct neural networks from GPs, where one expected the neural networks to approximately only allow solutions to the differential equations as trained functions.

The papers [48–59] constructs priors for a subset of our class of ODEs and an even smaller subset of our class of PDEs, the so-called latent force models. Relevant systems are of the specific form $Af = Bg$ for diagonal matrices with entries in $\mathbb{R}[\partial_t]$ and a linear operator matrix B not containing ∂_t .

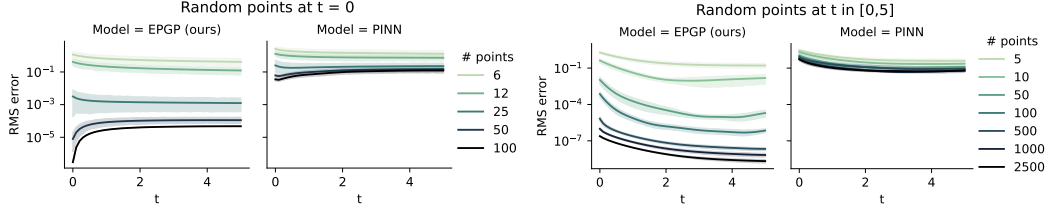


Figure 2: Comparison of the error between EPGP (ours) and PINN, for the cases when training data is constrained to $t = 0$ (left) and spread over the entire interval $t \in [0, 5]$ (right). EPGP yields considerably better results over a wide range of the amount of training data. The error bars stem from training the model on 10 different instances.

Using Green’s operator, the matrix A can be “inverted” at the cost of an integral on the right hand side. This yields a system that is controllable in the sense of [17], and hence it can be parametrized. Usually, but not necessarily, only the marginalization over f is being used and g considered “latent”. The priors from latent force models are different then ours, but are equivalent in the sense of dominating each other after some assumptions and restrictions have been made. These approaches are special cases of [18], which constructs covariance functions for any linear system of ODEs with constant coefficients using the Smith form of operator matrices. Notably, [60] used these methods in the context of linearization.

GP are a classical tool for purely data based simulation model. Hence, they also appear regularly with their standard covariance functions as an approximate model inside various models working with differential equations [61–66, 46, 67]. Furthermore, a huge class of probabilistic ODE solvers [68–75] and a smaller class of probabilistic PDE solvers [76–78] make use of GPs when dealing with non-linear differential equations, but do not construct new covariance functions specifically for differential equations. For systems of PDEs, solutions can be propagated forward in time using numerical discretization combined with GPs [79].

Differential equations are often used together with boundary conditions. There is recent interest in constructing GP priors encoding such boundary conditions [80–83] and even work constructing GP priors combining differential equations with boundary conditions [24, 25].

6 Examples

6.1 Heat equation

The one-dimensional heat equation is given by the PDE $\partial_x^2 u(x, t) = \partial_t u(x, t)$. Our first goal is to infer the exact solution

$$u(x, t) = \frac{\sqrt{5}(64t^3 + 125(-3 + x)(-1 + x)(2 + x) - 50t(-2 + x)(13 + 4x) + 40t^2(16 + 5x))}{e^{x^2/(5+4t)}(5 + 4t)^{7/2}}$$

purely from sampled data points, without any knowledge about boundary conditions. Consider the domain $(x, t) \in [-5, 5] \times [0, 5]$ on a 101×51 grid of equally spaced points. These 5151 corresponding function values serve as our “underlying truth”.

We compare our method with PINN [37] in two setups. First, we test the models’ ability to solve the heat equation given initial data. Therefore, we train on different numbers randomly chosen points at $t = 0$, and study the mean square error over all time points $t \in [0, 5]$. In our second setup, we test the models’ ability to interpolate the underlying true solution from a limited set of data scattered throughout time. We train on different numbers points chosen uniformly at random over the 101×51 grid. The results are depicted in Figure 2. The GP achieves an error several orders of magnitude smaller than the errors of PINN, even with fewer data points. In addition, there is a drastic difference in total computation time between EPGP (10s) and PINN (2h) using an Nvidia A100 GPU.

Next, we apply the EPGP to the 2D heat equation, with an added scale parameter on the Gaussian measure as discussed in the end of Section 4.1. The initial data is given at $t = 0$, on a 101×101 grid in the square $[-5, 5]^2$, where every value is equal to 0, except for a region depicting a smiling face

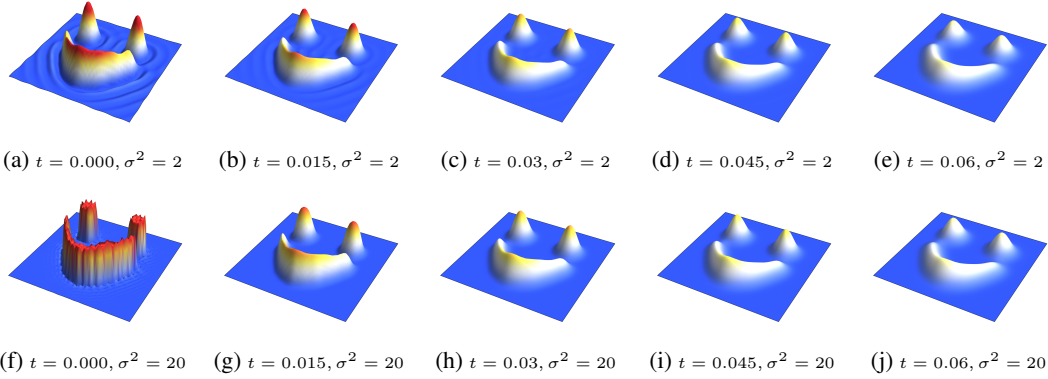


Figure 3: Heat dissipation in 2D at 5 timepoints, with scale parameters $\sigma^2 = 2$ and 20. The parameter σ^2 in the Gaussian measure regulates how strongly the learned function follows the initial data, depicted in Figure 7.

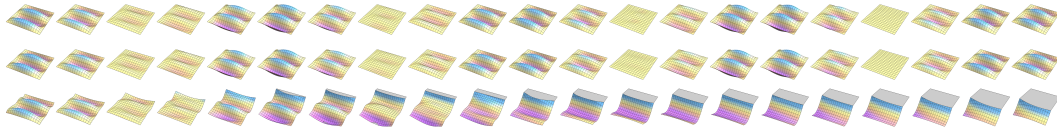


Figure 4: Solutions to wave equations for $t \in [0, 1]$. The top row shows a numerical solution, the first three frames of which serve as the training data. The second row is the mean from EPGP (ours), and the third row is the solution from by PINN. The gray regions in the PINN solutions are values > 0.3 .

where we set the value to 1. In this case, the scaling factor σ^2 in the covariance kernel determines how strongly the initial data is respected. Figure 3 compares the posterior mean at five timepoints. When $\sigma^2 = 20$, the prior allows abrupt changes, and the inferred function conforms to the jagged edges in the data. In contrast, for $\sigma^2 = 2$ the prior prefers smooth interpretations of the initial data. In both cases we show the instantaneous smoothing behavior at times $t > 0$, which is characteristic to solutions of the heat equation.

For details (covariance functions, experimental setup, etc.) and additional comparisons about the heat equation see Appendix D.

6.2 2D wave equation

Consider the 2D wave equation, given by $\frac{\partial^2 z}{\partial x^2} + \frac{\partial^2 z}{\partial y^2} = \frac{\partial^2 z}{\partial t^2}$. The solution we are trying to learn is obtained by solving the wave equation numerically, subject to boundary conditions $z(0, y, t) = z(1, y, t) = z(x, 0, t) = z(x, 1, t) = 0$, and initial conditions $z(x, y, 0) = \sin(4\pi x)y(1 - y)$, and $\frac{\partial z}{\partial t}(x, y, 0) = 0$. A plot of the numerical solution can be found on the top row of Figure 4.

To learn the numerical solution, we split the domain $(x, y, t) \in [0, 1]^3$ into a $21 \times 21 \times 21$ grid, and use the first three time values $t = 0, 0.05, 0.1$ as our training data. Thus the training set consists of 1323 points. For S-EPGP, we use a sum of 16 Dirac delta kernels, whose positions we will learn. This will act as a proxy for the Ehrenpreis-Palamodov measure. A PINN model, with 15 hidden layers of size 200, was also trained on the same data, but we failed to get adequate extrapolation performance. The bottom row of Figure 4 contains a PINN instance trained for 200,000 epochs. Technical details about wave equation and our experimental setup can be found in Appendix E.

6.3 Maxwell

The homogeneous Maxwell equations in a vacuum are

$$\nabla \cdot \mathbf{E} = 0, \quad \nabla \times \mathbf{E} = -\frac{\partial \mathbf{B}}{\partial t}, \quad \nabla \cdot \mathbf{B} = 0, \quad \nabla \times \mathbf{B} = \frac{\partial \mathbf{E}}{\partial t},$$

Table 1: Root mean square errors learning an exact solution to Maxwell’s equations, using different number of datapoints for training. Top: S-EPGP, with a varying number of Dirac delta measures. Bottom: PINN. Here HLW stands for “hidden layer width”.

Deltas	5 datapoints	10 datapoints	50 datapoints	100 datapoints	1000 datapoints
24	6.08 ± 0.797	8.92 ± 1.87	1.38 ± 0.698	0.981 ± 0.361	0.884 ± 0.347
48	4.31 ± 0.431	6.98 ± 1.37	0.356 ± 0.392	0.11 ± 0.101	0.0298 ± 0.0295
96	4.21 ± 0.387	3.81 ± 0.747	0.173 ± 0.169	0.00521 ± 0.00221	0.00192 ± 0.00203
192	3.9 ± 0.302	3.21 ± 0.706	1.22 ± 0.696	0.027 ± 0.0291	0.00239 ± 0.00155
384	3.45 ± 0.364	2.4 ± 0.796	0.192 ± 0.193	0.00974 ± 0.0113	0.000469 ± 0.00017
HLW	5 datapoints	10 datapoints	50 datapoints	100 datapoints	1000 datapoints
50	4.71 ± 0.403	4.09 ± 0.781	1.05 ± 0.304	0.742 ± 0.36	0.1 ± 0.0415
100	4.63 ± 0.469	4.12 ± 0.783	1.03 ± 0.278	0.693 ± 0.31	0.0948 ± 0.0272
200	4.72 ± 0.42	4.1 ± 0.789	1.06 ± 0.281	0.73 ± 0.296	0.0924 ± 0.0237

where $\mathbf{E} = (E_x(x, y, z, t), E_y(x, y, z, t), E_z(x, y, z, t))^T$ is the vector field corresponding to the electric field, and $\mathbf{B} = (B_x(x, y, z, t), B_y(x, y, z, t), B_z(x, y, z, t))^T$ is the vector field corresponding to the magnetic field.

We run the S-EPGP algorithm using $m = 4, 8, 16, 32,$ and 64 Dirac delta measures for each of the six multipliers. Each run is optimized using the Adam optimizer with learning rate 0.01 over 10000 epochs. Each experiment is repeated 10 times, and root mean squared errors of our predictions, along with the total number of Dirac delta measures used, are reported in Table 1.

For comparison, we repeat the experiment with PINN. Here too we base our PINN parameters on [84]. We use 5 hidden layers of varying sizes, with the \tanh activation function. PDE fit is measured using 500 collocation points sampled uniformly in the region $[-1, 1]^3 \times [0, 2]$. The loss function is defined as the sum of the mean squared error at the data points, and the mean square error of the PDE constraints, similarly to the original PINN paper [37]. We train the model for 9000 epochs using the Adam optimizer with learning rate 10^{-3} , and finally 1000 epochs using the L-BFGS optimizer. Results are reported in Table 1.

We immediately notice that the S-EPGP method manages to learn the true underlying solution much better than PINN, achieving root mean squared errors several orders of magnitude smaller even with a relatively small number of Dirac delta measures on the variety. We also note that the runtimes for S-EPGP scale well, and tend to outperform PINN. Our fastest S-EPGP model, with 24 Dirac deltas trained on only 5 points, completes 10000 training epochs in about 60 seconds on an Nvidia A100 GPU, whereas the slowest one, with 384 Dirac deltas trained on 1000 points, takes about 70 seconds to complete 10000 epochs. In comparison, each of the PINN models took about 200 seconds to complete 10000 epochs on the same GPU.

The details about calculating the Noetherian multipliers, characteristic variety and implementation of S-EPGP can be found in Appendix F.

7 Discussion

Our approach takes a starkly different approach to solving and learning PDE compared to other physics informed machine learning methods such as PINN. As is common in applied non-linear algebra [85], our philosophy is to remain in the exact setting as far as possible. This is evidenced by the application of exact symbolic algebraic techniques and the Ehrenpreis-Palamodov Fundamental Principle in the construction of our kernels. Thus we say that (S-)EPGP is physics *constrained*, as all realizations from our GPs are, by construction, exact solutions to the PDE system. Our experiments show the exact approach to be the superior and scalable, in both interpolation (learning) and extrapolation (solving) tasks. Non-exactness in the form of noise is only introduced at the very last step as we formulate the GP. Unlike PINN, this make the (S-)EPGP training objective statistically well motivated, and enables the usage of other well established techniques for sparse, variational, and approximate GPs.

Compared to other methods of learning and solving PDE, our method is also more data-driven and algorithmic. We do not for example distinguish the time dimension from other spatial dimensions, as is often done in numerical methods. Our method also does not require explicit initial and boundary conditions: data points can be given anywhere in the domain, and can consist of function values, derivatives, or any combination thereof. For vector-valued functions, we can even learn on partial representations of the data, for example learning a solution to Maxwell’s equations from just the electric field data in order to infer a magnetic field. This makes (S-)EPGP extremely flexible and applicable with minimal domain expertise.

References

- [1] Carl Edward Rasmussen and Christopher K. I. Williams. *Gaussian processes for machine learning*. MIT Press, Cambridge, MA, 2006. ISBN 978-0-262-18253-9.
- [2] Silja Thewes, Markus Lange-Hegermann, Christoph Reuber, and Ralf Beck. Advanced Gaussian Process Modeling Techniques. In *Design of Experiments (DoE) in Powertrain Development*, 2015.
- [3] David Duvenaud. *Automatic model construction with Gaussian processes*. PhD thesis, University of Cambridge, 2014.
- [4] Christian Steinruecken, Emma Smith, David Janz, James Lloyd, and Zoubin Ghahramani. The automatic statistician. In *Automated Machine Learning*, pages 161–173. Springer, Cham, 2019.
- [5] Fabian Berns, Markus Lange-Hegermann, and Christian Beecks. Towards Gaussian processes for automatic and interpretable anomaly detection in industry 4.0. In *Proceedings of the International Conference on Innovative Intelligent Industrial Production and Logistics – IN4PL*, 2020.
- [6] Tanja Hernández Rodríguez, Anton Sekulic, Markus Lange-Hegermann, and Björn Frahm. Designing robust biotechnological processes regarding variabilities using multi-objective optimization applied to a biopharmaceutical seed train design. *Processes*, 10(5):883, 2022.
- [7] Christoph Zimmer, Mona Meister, and Duy Nguyen-Tuong. Safe active learning for time-series modeling with Gaussian processes. In *Advances in Neural Information Processing Systems*, 2018.
- [8] Peter S Swain, Keiran Stevenson, Allen Leary, Luis F Montano-Gutierrez, Ivan BN Clark, Jackie Vogel, and Teuta Pilizota. Inferring time derivatives including cell growth rates using gaussian processes. *Nature communications*, 7(1):1–8, 2016.
- [9] Heather A Harrington, Kenneth L Ho, and Nicolette Meshkat. Differential algebra for model comparison. *arXiv preprint arXiv:1603.09730*, 2016.
- [10] Ives Macêdo and Renner Castro. Learning Divergence-free and Curl-free Vector Fields with Matrix-valued Kernels. *Instituto Nacional de Matematica Pura e Aplicada, Brasil, Tech. Rep.*, 2008.
- [11] Michael Scheuerer and Martin Schlather. Covariance models for divergence-free and curl-free random vector fields. *Stoch. Models*, 28(3):433–451, 2012. ISSN 1532-6349. doi: 10.1080/15326349.2012.699756. URL <https://doi.org/10.1080/15326349.2012.699756>.
- [12] Niklas Wahlström, Manon Kok, Thomas B. Schön, and Fredrik Gustafsson. Modeling Magnetic Fields using Gaussian Processes. In *Proceedings of the 38th International Conference on Acoustics, Speech, and Signal Processing (ICASSP)*, 2013.
- [13] Arno Solin, Manon Kok, Niklas Wahlström, Thomas B Schön, and Simo Särkkä. Modeling and Interpolation of the Ambient Magnetic Field by Gaussian Processes. *IEEE Transactions on Robotics*, 2018.
- [14] Carl Jidling, Johannes Hendriks, Niklas Wahlström, Alexander Gregg, Thomas B Schön, Christopher Wensrich, and Adrian Wills. Probabilistic Modelling and Reconstruction of Strain. *Nuclear Instruments and Methods in Physics Research Section B: Beam Interactions with Materials and Atoms*, 2018.

- [15] Simo Särkkä. Linear Operators and Stochastic Partial Differential Equations in Gaussian Process Regression. In *International Conference on Artificial Neural Networks*. Springer, 2011.
- [16] Carl Jidling, Niklas Wahlström, Adrian Wills, and Thomas B Schön. Linearly Constrained Gaussian Processes. In *Advances in Neural Information Processing Systems*, 2017.
- [17] Markus Lange-Hegermann. Algorithmic Linearly Constrained Gaussian Processes. In *Advances in Neural Information Processing Systems*. 2018.
- [18] Andreas Besginow and Markus Lange-Hegermann. Constraining Gaussian Processes to Systems of Linear Ordinary Differential Equations. In *Advances in Neural Information Processing Systems*. 2022.
- [19] Justin Chen, Yairon Cid-Ruiz, Marc Härkönen, Robert Krone, and Anton Leykin. Noetherian operators in Macaulay2. *arXiv preprint arXiv:2101.01002*, 2021.
- [20] Yairon Cid-Ruiz, Roser Homs, and Bernd Sturmfels. Primary ideals and their differential equations. *Found. Comput. Math.*, 21(5):1363–1399, 2021. ISSN 1615-3375. doi: 10.1007/s10208-020-09485-6. URL <https://doi.org/10.1007/s10208-020-09485-6>.
- [21] Yairon Cid-Ruiz and Bernd Sturmfels. Primary decomposition with differential operators. *arXiv preprint arXiv:2101.03643*, 2021.
- [22] Justin Chen and Yairon Cid-Ruiz. Primary decomposition of modules: a computational differential approach. *Journal of Pure and Applied Algebra*, page 107080, 2022. ISSN 0022-4049. doi: <https://doi.org/10.1016/j.jpaa.2022.107080>. URL <https://www.sciencedirect.com/science/article/pii/S0022404922000767>.
- [23] Rida Ait El Manssour, Marc Härkönen, and Bernd Sturmfels. Linear PDE with constant coefficients. *Glasgow Mathematical Journal, First View*, 2021. doi: 10.1017/S0017089521000355.
- [24] Markus Lange-Hegermann. Linearly constrained Gaussian processes with boundary conditions. In *International Conference on Artificial Intelligence and Statistics*. PMLR, 2021.
- [25] Markus Lange-Hegermann and Daniel Robertz. On boundary conditions parametrized by analytic functions. In François Boulier, Matthew England, Timur M. Sadykov, and Evgenii V. Vorozhtsov, editors, *Computer Algebra in Scientific Computing*, pages 225–245, Cham, 2022. Springer International Publishing.
- [26] Leon Ehrenpreis. *Fourier analysis in several complex variables*. Pure and Applied Mathematics, Vol. XVII. Wiley-Interscience [A division of John Wiley & Sons, Inc.], New York-London-Sydney, 1970.
- [27] V. P. Palamodov. *Linear differential operators with constant coefficients*. Die Grundlehren der mathematischen Wissenschaften, Band 168. Springer-Verlag, New York-Berlin, 1970. Translated from the Russian by A. A. Brown.
- [28] Lars Hörmander. *An introduction to complex analysis in several variables*, volume 7 of *North-Holland Mathematical Library*. North-Holland Publishing Co., Amsterdam, third edition, 1990. ISBN 0-444-88446-7.
- [29] J.-E. Björk. *Rings of differential operators*, volume 21 of *North-Holland Mathematical Library*. North-Holland Publishing Co., Amsterdam-New York, 1979. ISBN 0-444-85292-1.
- [30] Daniel R. Grayson and Michael E. Stillman. Macaulay2, a software system for research in algebraic geometry. Available at <http://www.math.uiuc.edu/Macaulay2/>.
- [31] Andrew Wilson and Ryan Adams. Gaussian process kernels for pattern discovery and extrapolation. In *International conference on machine learning*, pages 1067–1075. PMLR, 2013.
- [32] Miguel Lázaro-Gredilla, Joaquin Quiñero-Candela, Carl Edward Rasmussen, and Aníbal R. Figueiras-Vidal. Sparse spectrum gaussian process regression. *Journal of Machine Learning Research*, 11(63):1865–1881, 2010. URL <http://jmlr.org/papers/v11/lazaro-gredilla10a.html>.

- [33] David Eisenbud. *Commutative algebra*, volume 150 of *Graduate Texts in Mathematics*. Springer-Verlag, New York, 1995. ISBN 0-387-94268-8. doi: 10.1007/978-1-4612-5350-1. URL <https://doi.org/10.1007/978-1-4612-5350-1>.
- [34] Jean le Rond d’Alembert. Recherches sur la courbe que forme une corde tendue mise en vibration. *Memoires de l’Academie royale des sciences et belles lettres. Classe de mathematique.*, 3:214–219, 1747.
- [35] B Ph van Milligen, V Tribaldos, and JA Jiménez. Neural network differential equation and plasma equilibrium solver. *Physical review letters*, 75(20):3594, 1995.
- [36] Isaac E Lagaris, Aristidis C Likas, and Dimitris G Papageorgiou. Neural-network methods for boundary value problems with irregular boundaries. *IEEE Transactions on Neural Networks*, 11(5):1041–1049, 2000.
- [37] Maziar Raissi, Paris Perdikaris, and George E Karniadakis. Physics-informed neural networks: A deep learning framework for solving forward and inverse problems involving nonlinear partial differential equations. *Journal of Computational physics*, 378:686–707, 2019.
- [38] Salvatore Cuomo, Vincenzo Schiano Di Cola, Fabio Giampaolo, Gianluigi Rozza, Maizar Raissi, and Francesco Piccialli. Scientific machine learning through physics-informed neural networks: Where we are and what’s next. *arXiv preprint arXiv:2201.05624*, 2022.
- [39] Claudia Drygala, Benjamin Winhart, Francesca di Mare, and Hanno Gottschalk. Generative modeling of turbulence. *Physics of Fluids*, 34(3):035114, 2022.
- [40] Jiahao Zhang, Shiqi Zhang, and Guang Lin. Pagp: A physics-assisted gaussian process framework with active learning for forward and inverse problems of partial differential equations. *arXiv preprint arXiv:2204.02583*, 2022.
- [41] Jialei Chen, Zhehui Chen, Chuck Zhang, and CF Jeff Wu. Apik: Active physics-informed kriging model with partial differential equations. *SIAM/ASA Journal on Uncertainty Quantification*, 10(1):481–506, 2022.
- [42] Anne Dong. Kriging variables that satisfy the partial differential equation $\delta z = y$. In *Geostatistics*, pages 237–248. Springer, 1989.
- [43] Karl Gerald van den Boogaart. Kriging for processes solving partial differential equations. In *Proceedings of the 2001 Annual Conference of the International Association for Mathematical Geology, Cancun, Mexico*, pages 6–12, 2001.
- [44] Christopher G Albert. Gaussian processes for data fulfilling linear differential equations. *Multidisciplinary Digital Publishing Institute Proceedings*, 33(1):5, 2019.
- [45] Maziar Raissi, Paris Perdikaris, and George Em Karniadakis. Machine learning of linear differential equations using Gaussian processes. *Journal of Computational Physics*, 348:683–693, 2017.
- [46] Guofei Pang, Liu Yang, and George Em Karniadakis. Neural-net-induced gaussian process regression for function approximation and pde solution. *Journal of Computational Physics*, 384:270–288, 2019.
- [47] Sascha Ranftl. A connection between probability, physics and neural networks. In *Physical Sciences Forum*, volume 5, page 11. MDPI, 2022.
- [48] Mauricio Álvarez, David Luengo, and Neil D. Lawrence. Latent force models. In David van Dyk and Max Welling, editors, *Proceedings of the Twelfth International Conference on Artificial Intelligence and Statistics*, volume 5 of *Proceedings of Machine Learning Research*, pages 9–16, Hilton Clearwater Beach Resort, Clearwater Beach, Florida USA, 16–18 Apr 2009. PMLR. URL <https://proceedings.mlr.press/v5/alvarez09a.html>.
- [49] Jouni Hartikainen and Simo Sarkka. Sequential inference for latent force models. *arXiv preprint arXiv:1202.3730*, 2012.

- [50] Mauricio A Alvarez, David Luengo, and Neil D Lawrence. Linear latent force models using gaussian processes. *IEEE transactions on pattern analysis and machine intelligence*, 35(11): 2693–2705, 2013.
- [51] Steven Reece, Stephen Roberts, Siddhartha Ghosh, Alex Rogers, and Nicholas R Jennings. Efficient state-space inference of periodic latent force models. *Journal of Machine Learning Research*, 15:2337–2397, 2014.
- [52] Pablo A Alvarado, Mauricio A Alvarez, Genaro Daza-Santacoloma, Alvaro Orozco, and Germán Castellanos-Dominguez. A latent force model for describing electric propagation in deep brain stimulation: A simulation study. In *2014 36th Annual International Conference of the IEEE Engineering in Medicine and Biology Society*, pages 2617–2620. IEEE, 2014.
- [53] Siddhartha Ghosh, Steve Reece, Alex Rogers, Stephen Roberts, Areej Malibari, and Nicholas R Jennings. Modeling the thermal dynamics of buildings: A latent-force-model-based approach. *ACM Transactions on Intelligent Systems and Technology (TIST)*, 6(1):1–27, 2015.
- [54] Gustau Camps-Valls, Luca Martino, Daniel H Svendsen, Manuel Campos-Taberner, Jordi Muñoz-Marí, Valero Laparra, David Luengo, and Francisco Javier García-Haro. Physics-aware gaussian processes in remote sensing. *Applied Soft Computing*, 68:69–82, 2018.
- [55] Simo Särkkä, Mauricio A Alvarez, and Neil D Lawrence. Gaussian process latent force models for learning and stochastic control of physical systems. *IEEE Transactions on Automatic Control*, 64(7):2953–2960, 2018.
- [56] Rajdip Nayek, Souvik Chakraborty, and Sriram Narasimhan. A gaussian process latent force model for joint input-state estimation in linear structural systems. *Mechanical Systems and Signal Processing*, 128:497–530, 2019.
- [57] TJ Rogers, K Worden, and EJ Cross. On the application of gaussian process latent force models for joint input-state-parameter estimation: With a view to bayesian operational identification. *Mechanical Systems and Signal Processing*, 140:106580, 2020.
- [58] Elizabeth J Cross and Timothy J Rogers. Physics-derived covariance functions for machine learning in structural dynamics. *IFAC-PapersOnLine*, 54(7):168–173, 2021.
- [59] Paterne Gahungu, Christopher W Lanyon, Mauricio A Alvarez, Engineer Bainomugisha, Michael Smith, and Richard D Wilkinson. Adjoint-aided inference of gaussian process driven differential equations. *Advances in Neural Information Processing Systems*, 2022.
- [60] Wil Ward, Tom Ryder, Dennis Prangle, and Mauricio Alvarez. Black-box inference for non-linear latent force models. In *International Conference on Artificial Intelligence and Statistics*, pages 3088–3098. PMLR, 2020.
- [61] Kian Chai, Christopher Williams, Stefan Klanke, and Vijayakumar Sethu. Multi-task Gaussian process learning of robot inverse dynamics. *NeurIPS*, 2008.
- [62] Hongxu Zhao, Ran Jin, Su Wu, and Jianjun Shi. Pde-constrained gaussian process model on material removal rate of wire saw slicing process. *Journal of Manufacturing Science and Engineering*, 133(2), 2011.
- [63] Ilias Bilonis, Nicholas Zabararas, Bledar A Konomi, and Guang Lin. Multi-output separable Gaussian process: Towards an efficient, fully Bayesian paradigm for uncertainty quantification. *Journal of Computational Physics*, 241:212–239, 2013.
- [64] Edgar D Klenske, Melanie N Zeilinger, Bernhard Schölkopf, and Philipp Hennig. Gaussian process-based predictive control for periodic error correction. *IEEE Transactions on Control Systems Technology*, 24(1):110–121, 2015.
- [65] Selvakumar Ulaganathan, Ivo Couckuyt, Tom Dhaene, Joris Degroote, and Eric Laermans. Performance study of gradient-enhanced Kriging. *Engineering with computers*, 32(1):15–34, 2016.

- [66] Pankaj Kumar Rai and Shivam Tripathi. Gaussian process for estimating parameters of partial differential equations and its application to the richards equation. *Stochastic Environmental Research and Risk Assessment*, 33(8):1629–1649, 2019.
- [67] Yifan Chen, Bamdad Hosseini, Houman Owhadi, and Andrew M Stuart. Solving and learning nonlinear pdes with gaussian processes. *Journal of Computational Physics*, 447:110668, 2021.
- [68] Ben Calderhead, Mark Girolami, and Neil D Lawrence. Accelerating Bayesian inference over nonlinear differential equations with Gaussian processes. *NeurIPS*, 2009.
- [69] Michael Schober, David K Duvenaud, and Philipp Hennig. Probabilistic ODE solvers with Runge-Kutta means. *NeurIPS 2014*, 27, 2014.
- [70] Alonso Marco, Philipp Hennig, Jeannette Bohg, Stefan Schaal, and Sebastian Trimpe. Automatic LQR tuning based on Gaussian process optimization: Early experimental results. In *Second Machine Learning in Planning and Control of Robot Motion Workshop at International Conference on Intelligent Robots and Systems*, 2015.
- [71] Michael Schober, Simo Särkkä, and Philipp Hennig. A probabilistic model for the numerical solution of initial value problems. *Statistics and Computing*, 29(1):99–122, 2019.
- [72] Nicholas Krämer and Philipp Hennig. Linear-time probabilistic solution of boundary value problems. *NeurIPS*, 2021.
- [73] Filip Tronarp, Simo Särkkä, and Philipp Hennig. Bayesian ode solvers: The maximum a posteriori estimate. *Statistics and Computing*, 31(3):1–18, 2021.
- [74] Nathanael Bosch, Philipp Hennig, and Filip Tronarp. Calibrated adaptive probabilistic ODE solvers. In *AISTATS*, 2021.
- [75] Jonathan Schmidt, Nicholas Krämer, and Philipp Hennig. A probabilistic state space model for joint inference from differential equations and data. *NeurIPS 2021*, 34, 2021.
- [76] Ilias Bilionis. Probabilistic solvers for partial differential equations. *arXiv preprint arXiv:1607.03526*, 2016.
- [77] Jon Cockayne, Chris Oates, Tim Sullivan, and Mark Girolami. Probabilistic numerical methods for pde-constrained bayesian inverse problems. In *AIP Conference Proceedings*, volume 1853, page 060001. AIP Publishing LLC, 2017.
- [78] Nicholas Krämer, Jonathan Schmidt, and Philipp Hennig. Probabilistic numerical method of lines for time-dependent partial differential equations. In *International Conference on Artificial Intelligence and Statistics*, pages 625–639. PMLR, 2022.
- [79] Maziar Raissi, Paris Perdikaris, and George Em Karniadakis. Numerical gaussian processes for time-dependent and nonlinear partial differential equations. *SIAM Journal on Scientific Computing*, 40(1):A172–A198, 2018.
- [80] Matthias Hwai Yong Tan. Gaussian process modeling with boundary information. *Statist. Sinica*, 28(2):621–648, 2018. ISSN 1017-0405.
- [81] Arno Solin and Manon Kok. Know your boundaries: Constraining Gaussian processes by variational harmonic features. In *Proceedings of the 22nd International Conference on Artificial Intelligence and Statistics*. 2019.
- [82] Mamikon Gulian, Ari Frankel, and Laura Swiler. Gaussian process regression constrained by boundary value problems. *Comput. Methods Appl. Mech. Engrg.*, 388:Paper No. 114117, 18, 2022. ISSN 0045-7825. doi: 10.1016/j.cma.2021.114117. URL <https://doi.org/10.1016/j.cma.2021.114117>.
- [83] John Nicholson, Peter Kiessler, and D. Andrew Brown. A kernel-based approach for modelling Gaussian processes with functional information. *arXiv preprint arXiv:2201.11023*, 2022.

- [84] A. Mathews, M. Francisquez, J. W. Hughes, D. R. Hatch, B. Zhu, and B. N. Rogers. Uncovering turbulent plasma dynamics via deep learning from partial observations. *Phys. Rev. E*, 104: 025205, Aug 2021. doi: 10.1103/PhysRevE.104.025205. URL <https://link.aps.org/doi/10.1103/PhysRevE.104.025205>.
- [85] Mateusz Michalek and Bernd Sturmfels. *Invitation to nonlinear algebra*, volume 211 of *Graduate Studies in Mathematics*. American Mathematical Society, Providence, RI, 2021. ISBN 978-1-4704-5367-1.
- [86] Michalis Titsias. Variational learning of inducing variables in sparse gaussian processes. In David van Dyk and Max Welling, editors, *Proceedings of the Twelfth International Conference on Artificial Intelligence and Statistics*, volume 5 of *Proceedings of Machine Learning Research*, pages 567–574, Hilton Clearwater Beach Resort, Clearwater Beach, Florida USA, 16–18 Apr 2009. PMLR. URL <https://proceedings.mlr.press/v5/titsias09a.html>.
- [87] Marc Härkönen. *Dual representations of polynomial modules with applications to partial differential equations*. PhD thesis, Georgia Institute of Technology, May 2022. URI: <http://hdl.handle.net/1853/66629>.
- [88] Shiva Shankar. Controllability and vector potential: Six lectures at Steklov. *arXiv preprint arXiv:1911.01238*, 2019.

A Proof of Lemma 2.1

We will use the characterization of multivariate Gaussians in terms of characteristic functions (Fourier transform). Namely, the scalar random variables X_1, \dots, X_m are jointly Gaussian if and only if

$$\mathbb{E}[\exp(\sqrt{-1}\langle v, X \rangle)] = \exp(\sqrt{-1}(\langle v, \boldsymbol{\mu} \rangle - \frac{1}{2}\langle v, \boldsymbol{\Sigma}v \rangle)),$$

where $\boldsymbol{\mu}$ is the expectation of $X = (X_1, \dots, X_m)$ and $\boldsymbol{\Sigma}$ is the covariance matrix of X_i .

In our case X is given by the n vectors $(B_*g)(x_i)$, so $m = n\ell''$. Writing \mathbb{P} for the joint probability measure of $g(x_i)$ on $\mathbb{R}^{n\ell}$, we have for $v = (v_i)_{i=1}^n \in \mathbb{R}^{n\ell''}$,

$$\begin{aligned} \mathbb{E}[\exp(\sqrt{-1}\langle v, ((B_*g)(x_i))_{i=1}^n \rangle)] &= \mathbb{E}\left[\exp\left(\sqrt{-1}\sum_i \langle v_i, (B_*g)(x_i) \rangle\right)\right] \\ &= \int_{\mathbb{R}^{n\ell}} \exp\left(\sqrt{-1}\sum_i \langle v_i, By_i \rangle\right) d\mathbb{P}(y) \\ &= \int_{\mathbb{R}^{n\ell}} \exp\left(\sqrt{-1}\sum_i \langle B^T v_i, y_i \rangle\right) d\mathbb{P}(y) \\ &= \mathbb{E}\left[\exp\left(\sqrt{-1}\sum_i \langle B^T v_i, g(x_i) \rangle\right)\right] \\ &= \mathbb{E}[\exp(\sqrt{-1}\langle B^T v, (g(x_i))_{i=1}^n \rangle)], \end{aligned}$$

where the definition of B^T on $(\mathbb{R}^\ell)^n$ is extended by setting $B(v_i)_i = (Bv_i)_i$. To compute the expectation further, we set

$$\boldsymbol{\mu} = (\mu(x_i))_{i=1}^n \in \mathbb{R}^{n\ell}, \quad \boldsymbol{\Sigma} = (k(x_i, x_j))_{i,j=1}^n \in \mathbb{R}^{n\ell \times n\ell},$$

and obtain

$$\begin{aligned} \mathbb{E}[\exp(\sqrt{-1}\langle v, ((B_*g)(x_i))_{i=1}^n \rangle)] &= \exp(\sqrt{-1}(\langle B^T v, \boldsymbol{\mu} \rangle - \frac{1}{2}\langle B^T v, \boldsymbol{\Sigma}B^T v \rangle)) \\ &= \exp(\sqrt{-1}(\langle v, B\boldsymbol{\mu} \rangle - \frac{1}{2}\langle v, (B\boldsymbol{\Sigma}B^T)v \rangle)). \end{aligned}$$

From the last identity we infer that B_*g is a GP with mean $B\boldsymbol{\mu}$ and covariance $Bk(x, x')(B')^T$. \square

Comparing to [24, Lemma 2.2], we got rid of a compatibility assumption between probabilities and operators.

B Convergence of Ehrenpreis-Palamodov integrals

In general, integrals of the form

$$\int_V D(\mathbf{x}, \mathbf{z}) e^{\langle \mathbf{x}, \mathbf{z} \rangle} d\mu(\mathbf{z}),$$

appearing in the Ehrenpreis-Palamodov theorem need not converge. This makes the choice of measure μ slightly delicate. We propose three solutions.

1. If the variety $V \in \mathbb{C}^n$ is the affine cone of a projective variety, i.e. $x \in V \iff \lambda x \in V$ for all $\lambda \in \mathbb{C}$, we can restrict the measure to be supported on purely imaginary points, which equates to replacing V by $V \cap \sqrt{-1}\mathbb{R}^n$. This approach is used in the (S-)EPGP method.
2. In some cases, we may also need to restrict the domain of our solution. A concrete example is with the heat equation $\partial_x^2 = \partial_t$. The integral becomes $\int_{\mathbb{R}} e^{\sqrt{-1}ax - a^2t} d\mu(a)$. Here we want to restrict to $t \geq 0$, as this makes the integrand bounded.
3. A more general approach is to translate the exponent using the *supporting function* of a convex, compact set $\Omega \subseteq \mathbb{R}^n$, defined as

$$H_\Omega(\mathbf{z}) = \max_{\mathbf{y} \in \Omega} \langle \mathbf{z}, \mathbf{y} \rangle.$$

The integral is then modified to be

$$\int_V D(\mathbf{x}, \mathbf{z}) e^{\langle \mathbf{x}, \mathbf{z} \rangle} e^{-H_\Omega(\text{Re}(\mathbf{z}))} d\mu(\mathbf{z}).$$

This modification makes the real part of the exponent negative, which bounds the magnitude of the integrand whenever $\mathbf{x} \in \Omega$.

In all three cases, we may now choose μ to be any bounded measure. Thus convergence is guaranteed for EPGP and S-EPGP, which use Gaussian and Dirac delta measures respectively.

C Details about S-EPGP

In this section we derive the posterior distribution and training objective for S-EPGP. Recall that our latent functions are of the form

$$f(\mathbf{x}) = \sum_{j=1}^m \sum_{i=1}^r w_{i,j} \frac{1}{|S_{\mathbf{z}'_{i,j}}|} \left(\sum_{\mathbf{z} \in S_{\mathbf{z}'_{i,j}}} D_j(\mathbf{x}, \mathbf{z}) e^{\langle \mathbf{x}, \mathbf{z} \rangle} \right) =: \mathbf{w}^T \phi(\mathbf{x}),$$

where we assume $\mathbf{w} \sim \mathcal{N}(0, \frac{1}{mr}\Sigma)$.

Given n noisy observations $Y = f(X) + \epsilon$, where $\epsilon \sim \mathcal{N}(0, \sigma_0^2 I)$, the predictive distribution of $F_* = f(X_*)$ at new points X_* is given by

$$p(F_* | Y) = \mathcal{N}(\phi_*^H A^{-1} \Phi Y, \sigma_n^2 \phi_*^H A^{-1} \phi_*),$$

where $A = mr\sigma_0^2 \Sigma^{-1} + \Phi \Phi^H$, Φ is the $mr \times n$ matrix with columns $\phi(\mathbf{x})$ where \mathbf{x} is a training point, and ϕ_* is the $mr \times n_*$ matrix with columns $\phi(\mathbf{x}_*)$ for all n_* prediction points \mathbf{x}_* . Similarly, the log marginal likelihood is, up to a constant summand C

$$\log p(Y | \mathbf{x}, \theta) = -\frac{1}{2\sigma_0^2} (Y^T Y - Y^T \Phi^H A^{-1} \Phi Y) - \frac{n - mr}{2} \log \sigma_0^2 - \frac{1}{2} \log |\Sigma| - \frac{1}{2} \log |A| + C$$

Note the main bottleneck in the above computation is the inversion of A . Since usually $mr \ll n$, writing the training objective in this form is computationally efficient, since the matrix A has only size $mr \times mr$. Instead of inverting A , we compute a Cholesky decomposition, which also yields the determinant $|A|$.

D Details on the heat equation

The variety V corresponding to the heat equation is the parabola, which we will denote $z_x^2 = z_t$. The only multiplier D is 1. This can be confirmed using the Macaulay2 command `solvePDE`

```
i1 : needsPackage "NoetherianOperators";
i2 : R = QQ[x,t];
i3 : solvePDE ideal (x^2-t)
```

```
o3 = {{ideal(x^2 - t), {1 1 |}}}
```

We may choose z_x as the independent variable, which turns eq. (3) into the covariance function

$$\begin{aligned} k_{\text{EPGP}}(x, t, x', t') &= \int_{\mathbb{R}} e^{ixz_x - tz_x^2} e^{-ix'z_x - t'z_x^2} e^{-\frac{z_x^2}{2}} d\mathcal{L}(z_x) \\ &= \int_{\mathbb{R}} e^{iz_x(x-x') - (t+t'+1/2)z_x^2} e^{-ix'z_x - t'z_x^2} d\mathcal{L}(z_x) \end{aligned} \quad (4)$$

The integral converges whenever $t + t' + 1/2 > 0$, which is always the case in our domain. For the 1D heat equation, we approximate the integral using Monte-Carlo samples.

Our experimental setup for PINN is modeled after the one in [84]. We use 5 hidden layers, each of dimension, and a tanh activation function. The loss function is the sum of the mean squared error incurred from the training data, and the mean of the square of the value of the heat equation sampled at 100 random points on the domain $(x, t) \in [-5, 5] \times [0, 5]$. The neural network is trained for 10,000 epochs and parameters are optimized using Adam, with learning rate 10^{-4} .

For one particular instance, with the difference between the underlying truth see Figure 5. The benefit of using carefully crafted covariance functions is also clearly visible in Figure 6, which gathers total errors from all initial point setups in a comparison between EPGP and PINN.

For EPGP, the full 5151×5151 covariance matrix over 10,000 MC samples takes about one second to compute with an Nvidia A100 GPU. This is the main computational task in vanilla EPGP, which once completed, allow essentially instantaneous inference by posterior mean. This means that the entire experimental setup (10 repeats, 12 sets of initial points) takes about 10 seconds in total. In contrast, each PINN model takes about a minute to complete 10,000 epochs, and the computation has to be restarted from scratch for each set of initial points. The total time used to run the entire experimental setup using PINN is thus about two hours.

For the 2D heat equation, we use the EPGP kernel whose Gaussian measure includes a scale parameter σ^2 . In this case the EPGP covariance kernel becomes

$$k_{\sigma}(x, y, t; x', y', t') = \frac{1}{\frac{1}{\sigma^2} + 2(t+t')} e^{-\frac{(x-x')^2 + (y-y')^2}{2(\frac{1}{\sigma^2} + 2(t+t'))}}.$$

The initial data used in Figure 3 consists of the values $\{0, 1\}$ in the pattern shown in Figure 7. The initial data is given on a 101×101 grid of points in the range $(x, y) \in [-5, 5]^2$ and at time $t = 0$.

E Details about the wave equation

The Macaulay2 command `solvePDE` reveals that the characteristic variety for the 2D wave equation $\partial_x^2 + \partial_y^2 - \partial_t^2 = 0$ is the cone $x^2 + y^2 - t^2 = 0$, so each entry of ϕ in the S-EPGP kernel will have the form

$$\phi_j(x, y, t) = \frac{1}{2} \left(e^{\sqrt{-1}(xa_j + yb_j + t\sqrt{a_j^2 + b_j^2})} + e^{\sqrt{-1}(xa_j + yb_j - t\sqrt{a_j^2 + b_j^2})} \right)$$

where $j = 1, \dots, 16$. The spectral parameters $a_j, b_j \in \mathbb{R}$ are learned from the data.

We combined the S-EPGP kernel with a sparse variational GP, pioneered in [86]. We choose 32 inducing points and train for both the Dirac delta locations, variational inducing points simultaneously using the variational objective from [86]. All parameters were optimized using Adam with learning rate 10^{-2} for about 1000 epochs.

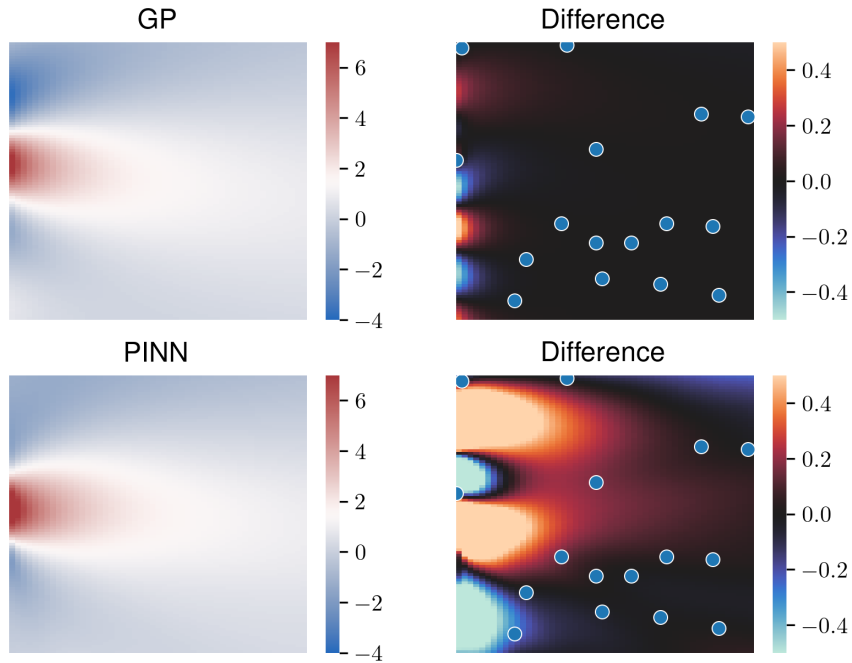


Figure 5: One set of trained instances with 16 randomly chosen datapoints. The vertical axis corresponds to x , and the horizontal axis corresponds to t , where $t = 0$ on the left and $t = 5$ on the right. The left plots describe the learned heat profile, and the right plot denotes the difference between the exact and the learned solution. We observe that PINN performs well in regions where the density of data points is high, such as in the bottom right of the picture, but its error is relatively large at small values of t .

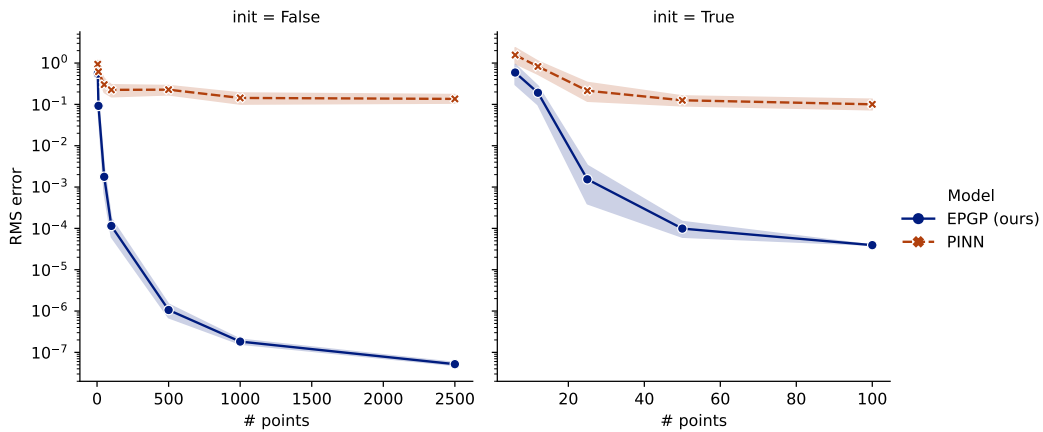


Figure 6: Aggregate plot of total errors with different choices of initial points. On the left ($\text{init} = \text{False}$), we choose training points at random in $t \in [0, 5]$. On the right ($\text{init} = \text{True}$), training points are chosen in $t = 0$.



Figure 7: Initial data for learning a solution to the heat equation in 2D. The dark data points correspond to a heat value of 0, and the light points correspond to a heat value of 1.

For PINN, we again follow a similar schedule to [84], with some fine-tuning. After a few attempts, we settled on 15 hidden layers, each of size 200. The neural network was trained using the Adam optimizer with learning rate 10^{-4} on 200,000 epochs. In our first attempts, we observed that PINN would converge to a constant solution, which almost certainly is a local optimum of the PINN loss function: a constant surely satisfies the wave equation equation exactly, but doesn't fit the data very well. This led us to reweight the PINN objective so that data fit was given a weight 1000 times larger than PDE fit. Despite our best efforts, we did not manage to get satisfactory extrapolation performance using PINN.

F Details about Maxwell's equation

If we set $\psi = (E_x, E_y, E_z, B_x, B_y, B_z)^T$, Maxwell's equations correspond to the following eight linear equations with constant coefficients:

$$\begin{bmatrix} \partial_x & \partial_y & \partial_z & 0 & 0 & 0 \\ 0 & -\partial_z & \partial_y & \partial_t & 0 & 0 \\ \partial_z & 0 & -\partial_x & 0 & \partial_t & 0 \\ -\partial_y & \partial_x & 0 & 0 & 0 & \partial_t \\ 0 & 0 & 0 & \partial_x & \partial_y & \partial_z \\ -\partial_t & 0 & 0 & 0 & -\partial_z & \partial_y \\ 0 & -\partial_t & 0 & \partial_z & 0 & -\partial_x \\ 0 & 0 & -\partial_t & -\partial_y & \partial_x & 0 \end{bmatrix} \psi = 0.$$

The output of the Macaulay2 command `solvePDE` returns two Noetherian multipliers and one variety, namely an affine cone of spheres.

```
i1 : needsPackage "NoetherianOperators"
i2 : R = QQ[x,y,z,t];
i3 : M = matrix {
      {x,y,z,0,0,0},
      {0,-z,y,t,0,0},
      {z,0,-x,0,t,0},
      {-y,x,0,0,0,t},
      {0,0,0,x,y,z},
      {-t,0,0,0,-z,y},
      {0,-t,0,z,0,-x},
      {0,0,-t,-y,x,0}
    };
i4 : solvePDE transpose M

o4 = {{ideal(x2 + y2 + z2 - t2), { | -xz |, | xy | }}
      { | -yz |, | y2-t2 | }
      { | -z2+t2 |, | yz | }
      { | -yt |, | -zt | }
      { | xt |, | 0 | }
      { | 0 |, | xt | }
```

We note that while the two operators are independent and generate the excess dual space [87], they are slightly "unbalanced", in the sense that the last two coordinates alone uniquely determine the two summands in the Ehrenpreis-Palamodov representation of the solution. Thus any potential noise in the y and z coordinates of the magnetic field will have a stronger effect on the quality of the inference procedure. We solve this imbalance by considering the kernel of the matrix as a map between free R/P modules, where $R = \mathbb{C}[x, y, z, t]$ is a polynomial ring, and $P = \langle x^2 + y^2 + z^2 - t^2 \rangle$ is the prime ideal corresponding to our characteristic variety. Since the generators of the kernel as an R/P -module maps to a set of $\text{frac}(R/P)$ -vector space generators, this procedure indeed yields a valid set of Noetherian multipliers [87]. This computation can also be carried out using Macaulay2.

```
i5 : N = coker transpose M;
i6 : P = first associatedPrimes N

          2      2      2      2
o6 = ideal(x  + y  + z  - t )

o6 : Ideal of R

i7 : kernel sub(M, R/P)

o7 = image {1} | xz      -y2-z2 xy      -yt      zt      0      |
             {1} | yz      xy      y2-t2 xt      0      -zt      |
             {1} | z2-t2 xz      yz      0      -xt      yt      |
             {1} | yt      0      -zt      xz      xy      -y2-z2 |
             {1} | -xt      zt      0      yz      y2-t2 xy      |
             {1} | 0      -yt      xt      z2-t2 yz      xz      |
```

We recognize our two Noetherian multipliers in the columns of the above matrix, as well as four extra operators. The six columns above will serve as our Noetherian multipliers D_1, \dots, D_6 in the S-EPGP method. This yields a slightly overparametrized, but also more balanced set of Noetherian multipliers, as every operator has a single zero in a distinct entry.

In order to avoid excessive subscripts, we will depart from our convention denoting primal (space-time) variables by the symbol \mathbf{x} and dual (spectral) variables by the symbol \mathbf{z} . Instead, we will use x, y, z, t for the space-time variables, and a, b, c, d for the corresponding spectral variables. Note that the symbols $\mathbf{x}, \mathbf{y}, \mathbf{z}, \mathbf{t}$ in the above matrix denoted by o7 actually correspond to $\partial_x, \partial_y, \partial_z, \partial_t$, and thus will be evaluated at the spectral points (a, b, c, d) on the variety $V = V(a^2 + b^2 + c^2 - d^2)$.

For the implicit parametrization trick, we let a, b, c be free variables, and solve for $d = \pm\sqrt{a^2 + b^2 + c^2}$. Thus, as described in Section 4.2, the S-EPGP kernel for Maxwell's equations will have the form

$$k(x, y, z, t; x', y', z', t') = \frac{1}{6m} \Phi(x, y, z, t)^H \Sigma \Phi(x', y', z', t'),$$

where $\Phi(x, y, z, t)$ is the $(6m \times 6)$ matrix whose rows, indexed by $i = 1, \dots, m$ and $j = 1, \dots, 6$ are

$$\begin{aligned} & \frac{1}{2} D_j(a_{ij}, b_{ij}, c_{ij}, \sqrt{a_{ij}^2 + b_{ij}^2 + c_{ij}^2})^T e^{\sqrt{-1}(a_{ij}x + b_{ij}y + c_{ij}z + \sqrt{a_{ij}^2 + b_{ij}^2 + c_{ij}^2}t)} + \\ & \frac{1}{2} D_j(a_{ij}, b_{ij}, c_{ij}, -\sqrt{a_{ij}^2 + b_{ij}^2 + c_{ij}^2})^T e^{\sqrt{-1}(a_{ij}x + b_{ij}y + c_{ij}z - \sqrt{a_{ij}^2 + b_{ij}^2 + c_{ij}^2}t)} \end{aligned}$$

Our goal is to infer an exact solution to Maxwell's equations from a set of 5, 10, 50, 100, and 1000 randomly selected datapoints in the range $(x, y, z, t) \in [-1, 1]^3 \times [0, 2]$. The exact solution is a superposition of five plane waves. Each plane wave is constructed by choosing two orthogonal

3-vectors $\mathbf{E}_{0,i}$ and \mathbf{k}_i . We then set

$$\begin{aligned}\mathbf{E}_i(x, y, z, t) &= \operatorname{Re} \left(\mathbf{E}_{0,i} e^{\sqrt{-1} \langle \mathbf{k}_i, (x,y,z) \rangle - \|\mathbf{k}_i\| t} \right) \\ \mathbf{B}_i(x, y, z, t) &= \frac{\mathbf{k}_i}{\|\mathbf{k}_i\|} \times \mathbf{E}_i(x, y, z, t) \\ \mathbf{E}(x, y, z, t) &= \sum_{i=1}^5 \mathbf{E}_i(x, y, z, t) \\ \mathbf{B}(x, y, z, t) &= \sum_{i=1}^5 \mathbf{B}_i(x, y, z, t).\end{aligned}$$

In our experiments, we choose

$$\begin{aligned}\mathbf{E}_{0,1} &= \begin{bmatrix} -2 \\ 0 \\ 1 \end{bmatrix} & \mathbf{E}_{0,2} &= \begin{bmatrix} 1 \\ 1 \\ 0 \end{bmatrix} & \mathbf{E}_{0,3} &= \begin{bmatrix} 1 \\ -1 \\ -1 \end{bmatrix} & \mathbf{E}_{0,4} &= \begin{bmatrix} 3 \\ 2 \\ 1 \end{bmatrix} & \mathbf{E}_{0,5} &= \begin{bmatrix} -7 \\ 2 \\ 3 \end{bmatrix} \\ \mathbf{k}_1 &= \begin{bmatrix} 1 \\ 0 \\ 2 \end{bmatrix} & \mathbf{k}_2 &= \begin{bmatrix} 0 \\ 0 \\ 1 \end{bmatrix} & \mathbf{k}_3 &= \begin{bmatrix} 0 \\ -1 \\ 1 \end{bmatrix} & \mathbf{k}_4 &= \begin{bmatrix} -1 \\ 1 \\ 1 \end{bmatrix} & \mathbf{k}_5 &= \begin{bmatrix} 0 \\ 3 \\ -2 \end{bmatrix}\end{aligned}$$

The exact function is then sampled on a uniform $11 \times 11 \times 11 \times 11$ grid in the ranges $(x, y, z) \in [-1, 1]^3$ and $t \in [0, 2]$.

G Affine subspaces

In this section, we consider the EPGP kernel in the special case where the characteristic variety V is an affine subspace, i.e. linear spaces and translations thereof.

We first show that our approach generalizes the approach to *parametrizable* systems of PDEs in [24]. The control theory literature calls such systems *controllable* [88]. Parametrizable systems are characterized by several algebraic conditions, but the one we are interested in is the following: controllable systems are precisely the ones where the *only* characteristic variety is \mathbb{C}^n . The Ehrenpreis-Palamodov fundamental principle thus implies that all solutions are of the form

$$f(\mathbf{x}) = \sum_i \int_{\mathbb{C}^n} D_i(\mathbf{z}) e^{\langle \mathbf{x}, \mathbf{z} \rangle} d\mu_i(\mathbf{z}) = \sum_i D_i(\partial_x) \int_{\mathbb{C}^n} e^{\langle \mathbf{x}, \mathbf{z} \rangle} d\mu_i(\mathbf{z}) =: \sum_i D_i(\partial_x) \phi_i(\mathbf{x}).$$

We can omit the \mathbf{x} -variables in the polynomials D_i , since every variable is independent over $R/(0)$, where the zero ideal (0) is the prime ideal corresponding to the variety \mathbb{C}^n [23, 87]. Furthermore, any choice of smooth functions $\phi_i(\mathbf{x})$ yields a solution. In other words, the set of solutions to the PDE $A(\partial_x)f = 0$ is the image of the matrix $B(\partial_x)$, which is the matrix with columns $D_i(\partial_x)$. Thus the EPGP kernel induces the pushforward GP of B , where our base covariance is the squared exponential in Example 4.1.

We now generalize this to general affine subspaces, i.e. translated linear spaces. Suppose A describes a system of linear PDEs whose only characteristic variety is an affine subspace. Then there is a parametrization of the variety of the form $z \mapsto Cz + b$ for some $n \times d$ constant matrix C of rank d and a constant vector b . By a change of variables, we may choose the Noetherian operators to be functions of \mathbf{z} only, so by Ehrenpreis-Palamodov the solution set consists of summands of the form

$$\begin{aligned}f_i(\mathbf{x}) &= \int_{\mathbb{C}^d} D_i(\mathbf{z}) e^{\langle \mathbf{x}, C\mathbf{z} \rangle + \langle \mathbf{x}, b \rangle} d\mu_i(\mathbf{z}) \\ &= e^{\langle \mathbf{x}, b \rangle} D_i(\partial_{C^T \mathbf{x}}) \int_{\mathbb{C}^d} e^{\langle C^T \mathbf{x}, \mathbf{z} \rangle} d\mu_i(\mathbf{z}) \\ &= e^{\langle \mathbf{x}, b \rangle} (D_i(\partial_y) \phi_i(y))_{y \rightarrow C^T \mathbf{x}},\end{aligned}$$

where $\phi_i(y)$ is an arbitrary, smooth d -variate function. By Ehrenpreis-Palamodov, *every* smooth solution arises this way.

If we gather all D_i inside a matrix B , the EPGP kernel (up to a scaling factor) becomes $k_{\text{EPGP}}(\mathbf{x}, \mathbf{x}') = e^{\langle \mathbf{x}, b \rangle} (B(\partial_y)\gamma(y, y')B^T(\partial_{y'}))_{y \rightarrow C^T \mathbf{x}} e^{\langle \mathbf{x}', b \rangle}$, where $\gamma(y, y')$ is the d -dimensional square exponential covariance. We observe that $k_{\text{EPGP}}(\mathbf{x}, \mathbf{x}')$ is (up to scaling) the covariance function of $f(\mathbf{x}) = e^{\langle \mathbf{x}, b \rangle} (B(\partial_y)g(y))_{y \rightarrow C^T \mathbf{x}}$, where $g(y)$ is a vector of independent GPs with squared exponential covariance. Since $f(\mathbf{x})$ is the general form of a solution to the PDE A , and realizations of GPs with squared exponential covariance functions are dense in the set of smooth functions, we conclude that our method constructs a kernel for which realizations are dense in the set of smooth solutions to A .